

Learning with Multiplicative Perturbations

Xiulong Yang, and Shihao Ji
Department of Computer Science
Georgia State University, Atlanta, GA, USA
xyang22@student.gsu.edu, sji@gsu.edu

Abstract

*Adversarial Training (AT) and Virtual Adversarial Training (VAT) are the regularization techniques that train Deep Neural Networks (DNNs) with adversarial examples generated by adding small but worst-case perturbations to input examples. In this paper, we propose xAT and xVAT, new adversarial training algorithms, that generate **multiplicative** perturbations to input examples for robust training of DNNs. Such perturbations are much more perceptible and interpretable than their **additive** counterparts exploited by AT and VAT. Furthermore, the multiplicative perturbations can be generated transductively or inductively while the standard AT and VAT only support a transductive implementation. We conduct a series of experiments that analyze the behavior of the multiplicative perturbations and demonstrate that xAT and xVAT match or outperform state-of-the-art classification accuracies across multiple established benchmarks while being about 30% faster than their additive counterparts. Furthermore, the resulting DNNs also demonstrate distinct weight distributions.*

1. Introduction

Over the past few years, Deep Neural Networks (DNNs) have achieved state-of-the-art performance on a wide range of learning tasks. However, the success of DNNs has a high reliance on large sets of labeled examples; when trained on small datasets, DNNs plague to overfitting if not regularized properly. For many practical applications, collecting a large amount of labeled examples is very expensive and/or time-consuming. To address this issue, researchers have investigated a host of techniques, such as Dropout [24], AT [4, 25], VAT [14], and Mixup [29], to regularize the training of DNNs. Such techniques usually augment the loss function of DNNs with a regularization term to prevent the model from overfitting when the labeled train set is small.

Several studies have found that the generalization performance of DNNs can be improved significantly by enforcing the prediction consistency of DNNs in response to

original inputs and their perturbed versions. For instance, Szegedy et al. [25] have found that very tiny perturbations to input samples (a.k.a., adversarial examples) can easily fool a well-trained DNN because the decision boundary of the DNN can change sharply around some data points. To improve the robustness of DNNs, they introduce AT to regularize the training of DNNs by augmenting the training set with adversarial examples. Furthermore, VAT [14, 15] extends the adversarial training principle of AT from supervised learning to semi-supervised learning by generating adversarial perturbations on unlabeled examples based on a divergence measure. However, the perturbations exploited by AT and VAT are *additive* in the sense that these perturbations are added pixel-wise to input examples.

In this paper, we propose a new type of perturbations called *multiplicative* perturbations that are generated via an L_0 -norm regularized optimization and *multiplied* to input examples pixel by pixel. This is in a stark contrast to the additive perturbations exploited by AT and VAT as the additive perturbations are generated by maximizing a divergence measure and *added* to input examples pixel by pixel. To illustrate the differences, Figure 1 demonstrates the learning pipelines of the additive perturbations and our multiplicative perturbations, with the main differences highlighted in the dashed boxes, where a pair of forward and backward propagations in the additive pipeline is replaced by a sparse mask generator in the multiplicative pipeline. Given an input image, the sparse mask generator outputs an adversarial mask, which is subsequently multiplied to the original input to generate a multiplicative adversarial example. We optimize the sparse mask generator adversarially to maximize a divergence measure under an L_0 -norm regularization. Similar to the additive perturbations, the multiplicative perturbations can be generated for labeled examples and unlabeled examples, and therefore can be used for supervised learning and semi-supervised learning. In light of the similarity to AT and VAT, we call our multiplicative AT and VAT as xAT and xVAT, with x denoting multiplication. In addition, our method can generate multiplicative perturbations transductively or inductively, while the additive perturba-

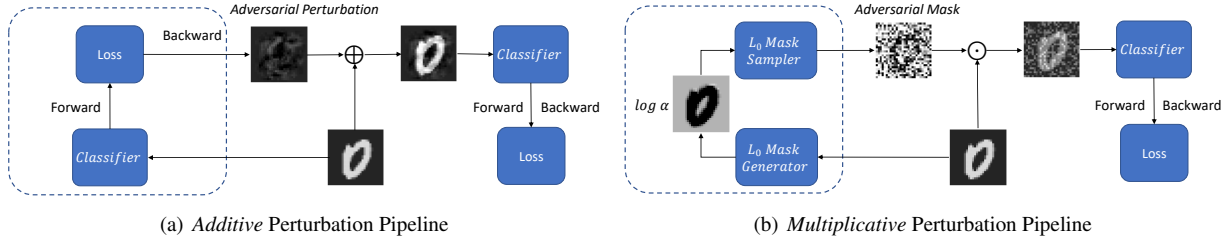


Figure 1. Comparison of the *additive* perturbation pipeline and the *multiplicative* perturbation pipeline.

tions exploited by AT and VAT are optimized transductively through backpropagation. For the reason to be discussed later, the parameters of sparse mask generator and the classifier of xAT and xVAT can be optimized simultaneously in one step, while AT and VAT have to optimize the additive perturbations and the classifier alternatively in two steps. As a result, xAT and xVAT are computationally more efficient than their additive counterparts. The main contributions of the paper are summarized as follows:

1. We introduce a new type of perturbations for robust training of DNNs that are multiplicative instead of additive; compared to the conventional additive perturbations, the multiplicative ones are much more perceptible and interpretable;
2. The multiplicative perturbations can be generated transductively or inductively, and the sparse mask generator and the classifier can be optimized simultaneously in one step, making xAT and xVAT computationally more efficient than their additive counterparts;
3. On four image classification benchmarks, xAT and xVAT match or outperform the state-of-the-art algorithms while being about 30% faster.

2. Method

Assume that we have a labeled dataset $\mathcal{D}_l = \{(\mathbf{x}_l^i, y_l^i), i = 1, 2, \dots, N_l\}$, and an unlabeled dataset $\mathcal{D}_u = \{\mathbf{x}_u^j, j = 1, 2, \dots, N_u\}$, where $\mathbf{x}^k \in \mathbb{R}^P$ denotes the k -th input sample and y^k is its corresponding label. We use $p(y|\mathbf{x}, \theta)$ to denote the output class distribution of a classifier, parameterized by θ , in response to an input \mathbf{x} . In supervised learning, we optimize model parameter θ by minimizing an empirical risk on \mathcal{D}_l , while in semi-supervised learning both \mathcal{D}_l and \mathcal{D}_u are utilized to optimize model parameter θ .

2.1. Additive Perturbations with AT and VAT

AT [4] and VAT [14] are two regularization techniques that have been proposed to generate small but worst-case perturbations for robust training of DNNs. Specifically,

AT [4] solves the following constrained optimization problem:

$$\mathcal{L}_{\text{AT}}(\mathbf{x}_l, y_l, \mathbf{r}_{\text{adv}}, \theta) = D[h(y_l|\mathbf{x}_l), p(y|\mathbf{x}_l + \mathbf{r}_{\text{adv}}, \theta)] \quad (1)$$

$$\text{with } \mathbf{r}_{\text{adv}} = \arg \max_{\mathbf{r}; \|\mathbf{r}\|_2 \leq \epsilon} D[h(y_l|\mathbf{x}_l), p(y|\mathbf{x}_l + \mathbf{r}, \theta)],$$

where $D[p, q]$ is a divergence measure between two distributions p and q . For the task of image classification, p and q are the probability vectors whose i -th element denotes the probability of an input image belonging to class i . In AT, D is the cross entropy loss $D[p, q] = -\sum_i p_i \log q_i$ and $h(y|\mathbf{x})$ is the one-hot encoding of label y for sample \mathbf{x} . Since $h(y|\mathbf{x})$ requires the true label y of \mathbf{x} , AT can only be applied to supervised learning. To extend the adversarial training to unlabeled samples, VAT [14] substitutes $h(y|\mathbf{x})$ with the predicted classification probability $p(y|\mathbf{x}, \theta)$ and solves a slightly different constrained optimization problem:

$$\mathcal{L}_{\text{VAT}}(\mathbf{x}_*, \mathbf{r}_{\text{adv}}, \theta) = D[p(y|\mathbf{x}_*, \theta), p(y|\mathbf{x}_* + \mathbf{r}_{\text{adv}}, \theta)] \quad (2)$$

$$\text{with } \mathbf{r}_{\text{adv}} = \arg \max_{\mathbf{r}; \|\mathbf{r}\|_2 \leq \epsilon} D[p(y|\mathbf{x}_*, \theta), p(y|\mathbf{x}_* + \mathbf{r}, \theta)],$$

where \mathbf{x}_* can be either labeled data \mathbf{x}_l or unlabeled data \mathbf{x}_u , and $D[p, q]$ is the KL divergence $D[p, q] = \sum_i p_i \log \frac{p_i}{q_i}$. Since no true label is required in the optimization above, VAT can be applied to both labeled and unlabeled data.

Figure 1(a) illustrates the general training pipeline of AT and VAT. Due to the constrained optimization in Eqs. 1 and 2, the exact closed-form solution of the adversarial perturbation \mathbf{r}_{adv} is intractable. Instead, fast approximation algorithms are proposed to estimate \mathbf{r}_{adv} iteratively. For AT, the adversarial perturbations can be approximated as:

$$\mathbf{r}_{\text{adv}} \approx \begin{cases} \epsilon \frac{\mathbf{g}}{\|\mathbf{g}\|_2} & L_2\text{-norm} \\ \epsilon \text{sign}(\mathbf{g}) & L_\infty\text{-norm,} \end{cases} \quad (3)$$

where $\mathbf{g} = \nabla_{\mathbf{x}_l} D[h(y|\mathbf{x}_l), p(y|\mathbf{x}_l, \theta)]$. And for VAT, the perturbation can be approximated via power iteration and estimated by:

$$\mathbf{r}_{\text{adv}} \approx \epsilon \frac{\mathbf{g}}{\|\mathbf{g}\|_2} \quad L_2\text{-norm,} \quad (4)$$

where $\mathbf{g} = \nabla_{\mathbf{r}} D[p(y|\mathbf{x}_*, \theta), p(y|\mathbf{x}_* + \mathbf{r}, \theta)]$. For both algorithms, backpropagation is needed to compute the additive perturbation \mathbf{r}_{adv} .

2.2. Multiplicative Perturbations

In contrast to the additive perturbations exploited by AT and VAT, we introduce a new type of perturbations that are multiplicative:

$$\mathbf{x}_{\text{xadv}} = \mathbf{x} \odot \mathbf{z}, \quad (5)$$

where $\mathbf{x} \in \mathbb{R}^P$ denotes an input image, $\mathbf{z} \in \{0, 1\}^P$ is a set of binary masks, and \odot is the element-wise multiplication. We can interpret $\mathbf{x} \odot \mathbf{z}$ as an operation that attaches a binary random variable z^j to each pixel j of \mathbf{x} , for all $j \in \{1, 2, \dots, P\}$. When $z^j = 0$, the corresponding pixel value is set to 0. Otherwise, the corresponding pixel value is retained without any changes. With the multiplicative perturbations, we have the following constrained optimization problem:

$$\mathcal{L}_{\text{xadv}}(\mathbf{x}, \mathbf{z}_{\text{xadv}}, \boldsymbol{\theta}) = D[p(y|\mathbf{x}, \boldsymbol{\theta}), p(y|\mathbf{x} \odot \mathbf{z}_{\text{xadv}}, \boldsymbol{\theta})] \quad (6a)$$

$$\text{with } \mathbf{z}_{\text{xadv}} = \arg \max_{\mathbf{z}} D[p(y|\mathbf{x}, \boldsymbol{\theta}), p(y|\mathbf{x} \odot \mathbf{z}, \boldsymbol{\theta})], \quad (6b)$$

where $D[p, q]$ adopts the cross entropy function for xAT, and the KL divergence for xVAT. To simplify the notation, we define

$$\Delta D(\mathbf{z}, \mathbf{x}, \boldsymbol{\theta}) = D[p(y|\mathbf{x}, \boldsymbol{\theta}), p(y|\mathbf{x} \odot \mathbf{z}, \boldsymbol{\theta})]. \quad (7)$$

In this formulation, $\mathbf{z}_{\text{xadv}} \in \{0, 1\}^P$ is optimized adversarially to maximize the divergence measure in Eq. 6b. This means that we wish z^j to take value of 0 if zeroing out the corresponding pixel j will make the prediction significantly different from the original prediction $p(y|\mathbf{x}, \boldsymbol{\theta})$. Apparently, a trivial solution of \mathbf{z} is all 0s, which is likely to maximize the divergence measure in Eq. 6b, but is catastrophic to the optimization of model parameter $\boldsymbol{\theta}$ in Eq. 6a. To avoid this detrimental solution, we augment Eq. 6b with the L_0 -norm of \mathbf{z} to regularize the learning of \mathbf{z} :

$$\begin{aligned} \mathbf{z}_{\text{xadv}} &= \arg \max_{\mathbf{z}} \Delta D(\mathbf{z}, \mathbf{x}, \boldsymbol{\theta}) + \lambda \|\mathbf{z}\|_0 \\ &= \arg \max_{\mathbf{z}} \Delta D(\mathbf{z}, \mathbf{x}, \boldsymbol{\theta}) + \lambda \sum_{j=1}^P \mathbb{1}_{[z^j \neq 0]} \end{aligned} \quad (8)$$

where $\mathbb{1}_{[c]}$ is an indicator function that outputs 1 if the condition c is satisfied, and 0 otherwise. Consider two extreme cases. When $\mathbf{z} = \mathbf{0}$, the first term ΔD is likely to reach its maximum, but the second term $\|\mathbf{z}\|_0$ is minimized to 0, and thus $\mathbf{z} = \mathbf{0}$ is unlikely to maximize Eq. 8. On the other hand, when $\mathbf{z} = \mathbf{1}$, the first term ΔD is minimized to 0 and the second term $\|\mathbf{z}\|_0$ reaches its maximum, and thus $\mathbf{z} = \mathbf{1}$ is unlikely to maximize Eq. 8 either. Therefore, a good solution must lie in between these two extremes, where some elements of \mathbf{z} are 0s and the remaining are 1s. As the training proceeds, the optimized \mathbf{z} might gradually become an adversarial mask that blocks salient regions of an image,

leads to an unreliable prediction and therefore maximizes Eq. 8. Subsequently, this adversarial mask will regularize the trained DNN from Eq. 6a to be robust to this multiplicative perturbation. We will demonstrate this behavior when we present results.

2.2.1 Stochastic Variational Optimization

To optimize Eq. 8, we need to compute its gradient w.r.t. \mathbf{z} . Since $\mathbf{z} \in \{0, 1\}^P$ is a set of binary random variables, both the first term and the second term of Eq. 8 are not differentiable. Hence, we resort to approximation algorithms to solve this binary optimization problem. Fortunately, we can use an inequality from stochastic variational optimization [2] to derive a lower-bound of Eq. 8. That is, given any function $\mathcal{F}(\mathbf{z})$ and any distribution $q(\mathbf{z})$, the following inequality holds:

$$\max_{\mathbf{z}} \mathcal{F}(\mathbf{z}) \geq \mathbb{E}_{\mathbf{z} \sim q(\mathbf{z})} [\mathcal{F}(\mathbf{z})] \quad (9)$$

i.e., the maximum of a function is lower bounded by the expectation of the function.

Since $z^j, j \in \{1, 2, \dots, P\}$ is a binary random variable, we assume z^j is subject to a Bernoulli distribution with parameter $\pi^j \in [0, 1]$, i.e. $q(z^j | \pi^j) = \text{Ber}(z^j; \pi^j)$. Thus, Eq. 8 can be lower bounded by its expectation:

$$\pi_{\text{xadv}} = \arg \max_{\boldsymbol{\pi}} \mathbb{E}_{q(\mathbf{z}|\boldsymbol{\pi})} [\Delta D(\mathbf{z}, \mathbf{x}, \boldsymbol{\theta})] + \lambda \sum_{j=1}^P \pi^j \quad (10)$$

Now the second term of Eq. 10 is differentiable w.r.t. the new model parameters $\boldsymbol{\pi}$. However, the first term is still problematic as the expectation over a large number of binary random variables \mathbf{z} is intractable and so is its gradient. Therefore, further approximations are required.

2.2.2 The Hard Concrete Gradient Estimator

There exist a number of gradient estimators to this stochastic binary optimization problem, such as REINFORCE [28], Gumbel-Softmax [7, 13], REBAR [27], RELAX [5] and the hard concrete estimator [12]. We resort to the hard concrete estimator to optimize Eq. 10 since it's straightforward to implement and demonstrates superior performance in our experiments. Specifically, the hard concrete gradient estimator employs a reparameterization trick to approximate the original optimization problem (10) by a close surrogate function:

$$\begin{aligned} \log \boldsymbol{\alpha}_{\text{xadv}} &= \arg \max_{\log \boldsymbol{\alpha}} \mathbb{E}_{\mathbf{u} \sim \mathcal{U}(0,1)} [\Delta D(g(f(\log \boldsymbol{\alpha}, \mathbf{u})), \mathbf{x}, \boldsymbol{\theta})] \\ &+ \lambda \sum_{j=1}^P \sigma \left(\log \alpha^j - \beta \log \frac{-\gamma}{\zeta} \right) \end{aligned} \quad (11)$$

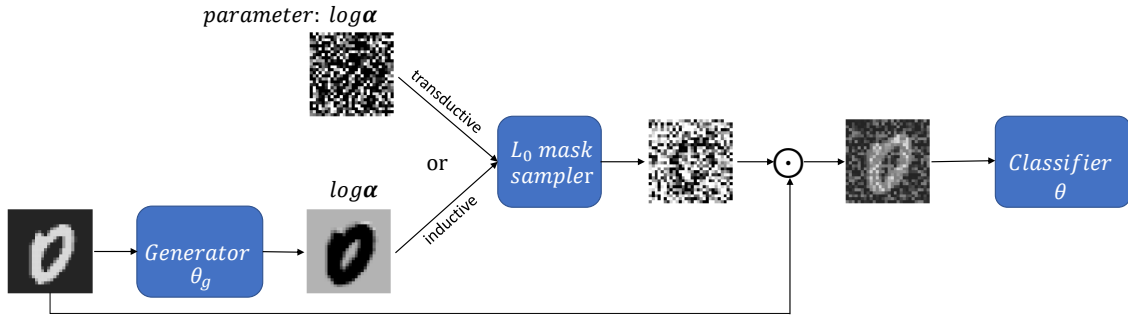


Figure 2. The pipeline of the transductive and inductive implementations of multiplicative adversarial training.

with

$$f(\log \alpha, \mathbf{u}) = \sigma((\log \mathbf{u} - \log(1 - \mathbf{u}) + \log \alpha) / \beta) (\zeta - \gamma) + \gamma, \\ g(\cdot) = \min(1, \max(0, \cdot)),$$

where $\mathcal{U}(0, 1)$ denotes the uniform distribution in the range of $[0, 1]$, $\sigma(t) = 1/(1 + \exp(-t))$ is the sigmoid function, and $\beta = 2/3$, $\gamma = -0.1$, and $\zeta = 1.1$ are the typical parameter values of the hard concrete distribution. For more details on the hard concrete gradient estimator, we refer the readers to [12]. With this reparameterization, the surrogate function (11) is now differentiable w.r.t. its parameters $\log \alpha \in \mathbb{R}^P$.

Once we have an optimized $\log \alpha_{\text{xadv}}$, we can sample an adversarial mask from the hard concrete distribution $q(\mathbf{z} | \log \alpha_{\text{xadv}})$ by

$$\hat{\mathbf{z}}_{\text{xadv}} = g(f(\log \alpha_{\text{xadv}}, \mathbf{u})), \quad \mathbf{u} \sim \mathcal{U}(0, 1). \quad (12)$$

We can then optimize model parameter θ by minimizing the following regularized empirical risk over all training samples:

$$\mathcal{L}(\theta) = \frac{1}{N_l} \sum_{(\mathbf{x}_l, y_l) \in \mathcal{D}_l} \mathcal{L}_{\text{ce}}(h(\mathbf{x}_l, \theta), y_l) \\ + \eta \frac{1}{N_l + N_u} \sum_{\mathbf{x} \in \{\mathcal{D}_l, \mathcal{D}_u\}} \mathcal{L}_{\text{xadv}}(\mathbf{x}, \hat{\mathbf{z}}_{\text{xadv}}, \theta), \quad (13)$$

where $h(\mathbf{x}_l, \theta)$ denotes the output of a classifier, parameterized by θ , \mathcal{L}_{ce} is the cross entropy loss over labeled training examples, and η is a regularization hyperparameter that balances the cross entropy loss \mathcal{L}_{ce} of labeled data and the adversarial training loss $\mathcal{L}_{\text{xadv}}$ of all training examples.

2.2.3 Transductive vs. Inductive Training

The optimization of the final loss function (13) can be implemented transductively or inductively. For a transductive implementation, we set $\log \alpha \in \mathbb{R}^P$ as model parameters to be optimized for each input example $\mathbf{x} \in \{\mathcal{D}_l, \mathcal{D}_u\}$. The learned $\log \alpha$ is then used to generate a sparse adversarial

mask $\hat{\mathbf{z}}_{\text{xadv}}$, and subsequently the training proceeds to evaluate the final loss (13). However, this approach can't generate masks for images never seen during training. A more appealing approach is the inductive implementation, which employs a generator to produce a sparse adversarial mask for any input example \mathbf{x} . To formulate the inductive training, we model the generator as a neural network, parameterized by θ_g , and given an input \mathbf{x} we define its output as $\log \alpha = G(\mathbf{x}, \theta_g)$, which is used subsequently to sample a sparse adversarial mask $\hat{\mathbf{z}}_{\text{xadv}}$. The pipeline of the two implementations is illustrated in Figure 2.

One advantage of xAT/xVAT over AT/VAT is that due to the hard concrete reparameterization, we can optimize (a) classifier parameter θ , and (b) the hard concrete parameter $\log \alpha$ (for transductive training) or the generator parameter θ_g (for inductive training) simultaneously in one step. This is not true for AT and VAT since both of them rely on back-propagation to optimize additive perturbations, while back-propagation through the perturbations produced by back-propagation is computationally unstable. Therefore, both AT and VAT resort to optimizing additive perturbations \mathbf{r}_{adv} and classifier parameter θ alternatively in two steps. Because of this advantage, xAT and xVAT are computationally more efficient than their additive counterparts. We will demonstrate this when we present results.

2.2.4 Shrink or Expand Multiplicative Perturbations

It is worth mentioning one potential issue of multiplicative perturbations. Consider the additive adversarial example $\mathbf{x} + \mathbf{r}_{\text{adv}}$ with $\mathbf{r}_{\text{adv}} \approx \epsilon \frac{\mathbf{g}}{\|\mathbf{g}\|_p}$ (where $p = 2$ or ∞), and the multiplicative adversarial example $\mathbf{x} \odot \mathbf{z}$ with $\mathbf{z} \in \{0, 1\}^P$. Apparently, these two types of perturbations have very distinct geometric interpretations w.r.t. input example \mathbf{x} . For additive perturbations, the approximation $\mathbf{r}_{\text{adv}} \approx \epsilon \frac{\mathbf{g}}{\|\mathbf{g}\|_p}$ indicates that all additive perturbations are generated exactly on the surface of a ball (or a box) centered at \mathbf{x} with a radius of ϵ , and no additive perturbations would appear inside the ball (see Figure 3(a)). On the other hand, the multiplicative perturbations do not have this characteristic. Since z^j is be-

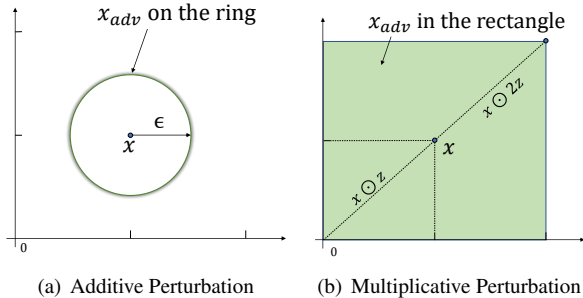


Figure 3. The effect of ϵ on different perturbations. (a) shows that the additive perturbations are on the surface of a ball with the radius ϵ . (b) demonstrates that our multiplicative perturbations are distributed within the rectangle.

tween 0 and 1, the admissible multiplicative perturbations can appear inside a box rather than only on the surface of a box (see Figure 3(b)). Note that the following inequality always holds:

$$\|x \odot z\| \leq \|x\|, \text{ with } z \in [0, 1]^P. \quad (14)$$

What does this mean is that the masked image $x \odot z$ is always darker than the original image x , which may be undesirable in some cases where the contrast of an image is low. To tackle this potential issue, we introduce a new parameter ϵ in the multiplicative formulation: $x \odot \epsilon z$. We only consider $\epsilon = 1$ or 2 in our experiments, while other positive values of ϵ are admissible. When $\epsilon = 1$, the masked images can only be darker than the original images, while when $\epsilon = 2$ the masked images can be darker or brighter as illustrated in Figure 3(b). Empirically, we find that $\epsilon = 1$ works reasonable well on all benchmark datasets in our experiments. We therefore don't tune it any further.

Comparing Figure 3(a) and Figure 3(b), it is clear that the solution space of multiplicative perturbations is much larger than that of additive perturbations. As we will show in the experiments, because of this difference, the trained DNNs from both perturbations demonstrate very distinct weight distributions.

3. Related Work

To improve the generalization of trained DNNs on unseen data examples, a variety of regularization techniques have been proposed in the past few years. Traditional regularization techniques impose an extra regularized term, such as the L_2 regularization or weight decay [6], to prevent the model from overfitting to a small set training examples. Dropout [24], a popular regularization technique, uniformly drops some hidden units from the network during training and is a model ensemble approach to avoiding overfitting.

Recently, a family of regularization techniques called consistency regularization has been proposed that encourages classifiers to yield consistent predictions on data sam-

ples and their perturbed versions. For example, the Π -Model [22] and STP [20] incorporate the following consistency loss

$$\|p(y|\text{Augment}_1(x), \theta) - p(y|\text{Augment}_2(x), \theta)\|_2^2 \quad (15)$$

as a regularizer for robust training of DNNs, where $\text{Augment}(x)$ represents a stochastically augmented version of x such that the two terms in Eq. 15 are not identical. Similarly, Temporal Ensembling [22], Mean Teacher [26] and fast-SWA [1] generate stochastic outputs by tracking the exponential moving average (EMA) of the past predictions and weights. Deep Co-Training [18] extends the consistency to an ensemble of models. Exploiting adversarial examples, AT and VAT compute small but worse-case perturbations as data augmentation, and encourage DNNs to produce consistent predictions on these samples. By combining the dropout and adversarial training, Park et al. [17] propose the adversarial dropout, which embeds an adversarial dropout layer to DNNs and optimizes the dropout mask adversarially to maximize the loss of DNNs. This work has a similar high-level idea to ours. However, their method works on much smaller last FC layer, and employs an expensive integer programming to solve the optimization problem. Because of these limitations, their technique cannot be applied to earlier but larger layers, while our xAT and xVAT operate at input layer with an L_0 -regularized binary optimization, which can be optimized efficiently via the hard concrete gradient estimator. Our experiments verify that xVAT not only demonstrates the state-of-the-art accuracies but also is about 30% faster than VAT, and therefore is much more scalable.

4. Experimental Results

We validate our xAT and xVAT on multiple public datasets with multiple network architectures for supervised learning and semi-supervised learning. Specifically, we illustrate how xVAT learns on a synthetic ‘‘moons’’ dataset [14]. We also demonstrate xAT and xVAT on four established image classification benchmarks: MNIST [10], SVHN [16], CIFAR-10 and CIFAR-100 [9]. Our main baselines are AT [4] and VAT [14, 15] since our work is primarily to investigate the effectiveness of multiplicative perturbations vs. additive perturbations. We also compare our methods with many state-of-the-art algorithms in terms of classification accuracy. For a fair comparison, we closely follow the experimental setup of VAT¹. All of our experiments are performed on NVIDIA Titan-Xp GPUs. We plan to release our PyTorch implementation to public to facilitate the research in this area.

¹https://github.com/takerum/vat_tf/

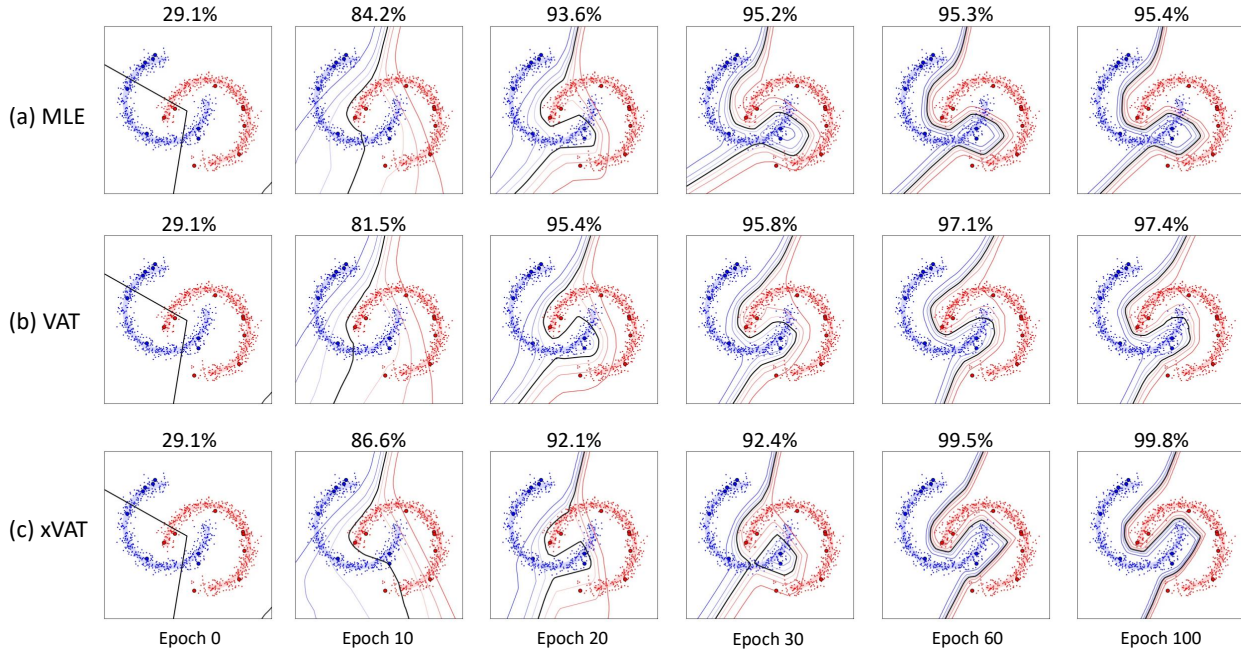


Figure 4. The evolution of the decision boundaries of MLE, VAT and xVAT on the synthetic “moons” dataset.

4.1. Synthetic Dataset

We first demonstrate the performance of xVAT on a synthetic “Moons” dataset [14]. The dataset contains 16 labeled training data points and 1000 test data points, uniformly distributed in two moon-shaped clusters for binary classification. We randomly select 500 test points as unlabeled training examples and use all 1000 test points for evaluation. We use an MLP with two hidden layers of 100 units. The input layer has 2 neurons corresponding to the 2-dim coordinates of each data point, which is transformed to a 100-dim vector by a fixed matrix. The output layer has two neurons for binary classification. The overall architecture of the MLP is 2-100 (fixed)-100-2 with the first weight matrix fixed. We compare the results of Maximum Likelihood Estimation (MLE) using the cross-entropy loss, VAT and xVAT. MLE only uses 16 labeled data points for supervised training, while VAT and xVAT use 16 labeled and 500 unlabeled data points for semi-supervised training. Figure 4 illustrates the evolution of the decision boundaries of MLE, VAT, xVAT on the “moons” dataset. As can be seen, xVAT yields a similar or slightly better decision boundary than that of VAT. Furthermore, both VAT and xVAT learn the decision boundaries that respect the underlying data manifold, demonstrating the effectiveness of multiplicative perturbations on this synthetic dataset.

4.2. Image Classification Benchmarks

We next evaluate xAT and xVAT on four established image classification benchmarks. Detailed description of the

benchmarks is provided in Appendix 6.1. Network architectures and experimental setup for reproducibility are provided in Appendix 6.2.

4.2.1 Semi-supervised Learning

For MNIST, we use an MLP with four hidden layers of 1200, 600, 300 and 150 units, respectively, which is the same architecture used in VAT [14, 15]. For SVHN, CIFAR-10 and CIFAR-100, the network architecture is a 13-layer CNN, the same as the one used in [15, 17, 22]. It is worth mentioning that for xAT and xVAT we normalize the MNIST images to $[-0.5, 0.5]$ rather than $[0, 1]$. This is because multiplicative perturbations have no effect on zero-valued pixels, while the MNIST images happen to have zero-valued black background, and therefore the $[-0.5, 0.5]$ normalization allows xAT/xVAT to generate valid multiplicative perturbations on the background of MNIST. On the other datasets, we adopt the same normalization approaches as in VAT. For the transductive implementation, we initialize the parameter $\log \alpha$ for each image with samples from a unit Gaussian distribution $\mathcal{N}(0, 1)$. For the inductive implementation, we use an one-layer CNN with one 3×3 filter as the generator. Interestingly, such a simple generator is sufficient to yield competitive results for all our experiments.

Tables 1 and 2 summarize the classification accuracies of xVAT on the four benchmark datasets as compared to the state-of-the-art algorithms. As we can see, xVAT achieves very competitive and sometimes even better accuracies than the state-of-the-arts, such as the II-model [22] and VAT.

Table 1. Test accuracies of semi-supervised learning algorithms on MNIST, SVHN and CIFAR-10. The results are averaged over 5 runs.

Method	Test Accuracy (%)		
	MNIST $N_l=100$	SVHN $N_l=1000$	CIFAR-10 $N_l=4000$
GAN with feature match [21]	99.07	91.89	81.37
CatGAN [23]	98.09	-	80.42
Ladder Networks [19]	98.94	-	79.60
Π -model [22]	-	94.57	83.45
Mean Teacher [26]	-	94.79	82.26
VAT [15]	98.64	94.23	85.18
xVAT (Transductive)	98.02	93.99	85.82
xVAT (Inductive)	97.82	94.22	86.59

Table 2. Test accuracies of semi-supervised learning algorithms on CIFAR-100. The results are averaged over 5 runs.

Method	Test Accuracy (%)
	$N_l=10000$
Supervised [22]	55.44
Π -model [22]	60.81
Temporal ensembling [22]	61.35
VAT [15]	59.71
xVAT (Transductive)	61.30
xVAT (Inductive)	61.76

Table 3. The training speeds of VAT and xVAT on the four benchmark datasets. The results are averaged over 5 runs.

Method	Seconds per epoch			
	MNIST	SVHN	CIFAR-10	CIFAR-100
VAT (ours)*	4.31	54.3	51.3	51.5
xVAT (Transductive)	4.54	36.6	34.1	39.3
xVAT (Inductive)	4.33	35.7	33.6	34.4

*For a fair comparison, we implement VAT in PyTorch and achieve similar accuracies as the official VAT implementation.

Furthermore, the inductive xVAT outperforms the transductive xVAT on 3 out of 4 benchmarks. This is likely because the per-image parameter $\log \alpha$ is more difficult to optimize than that of the shared generator parameter θ_g . Table 3 compares the per-epoch training speeds of VAT and xVAT. xVAT (both transductive and Inductive) is about 30% faster than VAT. This is because the generator of xVAT is significantly shallower than the CNN classifier, and therefore the multiplicative perturbations can be generated much more efficiently than the backpropagation-based additive perturbations. In general, VAT requires at least two pairs of forward

and backward propagations per iteration, while xVAT only needs one pair of forward and backward propagation, plus some extra time to update the parameter of generator. In our experiments, since an one-layer CNN generator is sufficient, which is significantly cheaper than the 13-layer CNN classifier, the cost of updating the generator is largely negligible, and therefore our xVAT is computationally more efficient than VAT. Because inductive xAT/xVAT in general outperform their transductive ones, in the experiments that follow we use inductive xAT/xVAT unless noted otherwise.

Table 4. Test accuracies of supervised learning on MNIST. The results are averaged over 5 runs.

Method	Test Accuracy (%)
Dropout [24]	98.95
Concrete Dropout [3]	98.60
Ladder networks [19]	99.43
Baseline (MLE) [15]	98.89
AT, L_∞ [15]	99.21
AT, L_2 [15]	99.29
VAT [15]	99.36
xAT (Inductive)	99.18
xVAT (Inductive)	99.08

Table 5. Test accuracies of supervised learning on CIFAR-10 and CIFAR-100. The results are averaged over 5 runs.

Method	Test Accuracy (%)	
	CIFAR-10	CIFAR-100
Baseline (MLE) [22]	93.24	73.58
Π -model [22]	94.44	73.68
Temporal ensembling [22]	94.40	73.70
AT, L_∞ (ours)*	93.90	74.04
VAT [15]	94.19	75.02
xAT (Inductive)	93.70	74.62
xVAT (Inductive)	93.88	75.30

*No reported results. For a fair comparison, we implement AT in PyTorch and verify its accuracies on MNIST, and report our results in the table.

4.2.2 Supervised Learning

We next evaluate the performance of xAT and xVAT in supervised learning on MNIST, CIFAR-10 and CIFAR-100. The same network architectures are used as in the experiments of semi-supervised learning. We compare the results of xAT and xVAT with the state-of-the-art algorithms in Tables 4 and 5. It is demonstrated that our xAT and xVAT achieve very competitive accuracies to the other competing methods, demonstrating the effectiveness of multiplicative perturbations in supervised learning.

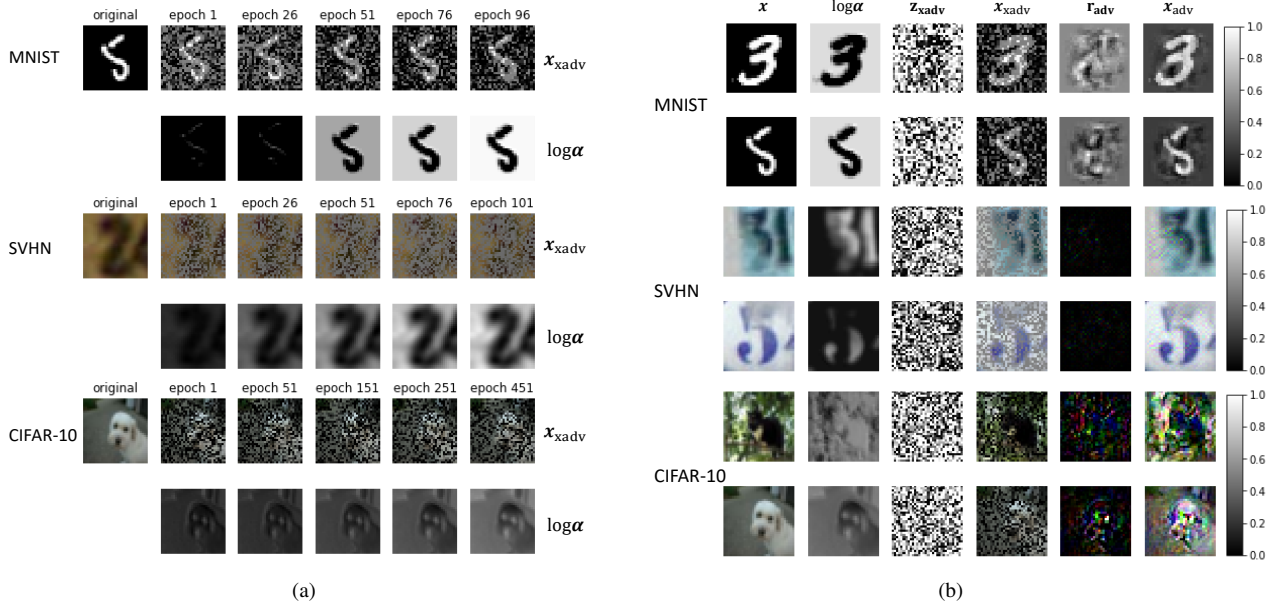


Figure 5. Visualization of multiplicative perturbations and additive perturbations from xVAT and VAT. (a) The evolution of $\log \alpha$ and x_{adv} during the training of xVAT on benchmark datasets. (b) Comparison of multiplicative and additive perturbations on example images from benchmark datasets.

4.3. Visualization of Multiplicative Perturbations

To understand the effectiveness of xVAT in generating multiplicative perturbations, we visualize the evolution of $\log \alpha$ and x_{adv} on example images from MNIST, SVHN and CIFAR-10, with the results shown in Figure 5(a). As we can see, at the beginning of the xVAT training, the output of sparse mask generator $\log \alpha$ isn't very informative as it generates multiplicative perturbations almost uniformly over the entire images. As the training proceeds and the sparse mask generator is trained adversarially, the mask learns to block the salient regions of the input images and leads to more effective adversarial examples. This can be observed from the learned $\log \alpha$ that gets more interpretable over training epochs.

To compare the multiplicative perturbations with the additive perturbations, Figure 5(b) illustrates their effects on example images from MNIST, SVHN and CIFAR-10. As we can see, visually these two types of perturbations are very different: the multiplicative perturbations are more perceptible than the additive counterparts, but the former are more interpretable than the latter as learned $\log \alpha$ clearly discover the salient regions of input images. It is worth mentioning that the higher visibility of the multiplicative perturbations is not a disadvantage of xAT/xVAT since our work is not to propose new adversarial attack algorithms but to investigate new adversarial training algorithms that can improve the robustness of DNNs. Evidently, our work demonstrates that multiplicative perturbations are *at least* as effective as additive perturbations at identifying the blind-

spots of DNNs and training on these perturbations can lead more robust DNNs.

4.4. Visualization of Weight Distributions from Different Algorithms

To investigate the differences of trained classifiers from different algorithms, we compare the model weights learned by MLE, VAT and xVAT on CIFAR-100. Figure 6 shows the histograms of model weights from three different CNN layers. It is demonstrated that xVAT learns a classifier whose weights have a much higher variance than those learned by VAT and MLE. In other words, xVAT learns a denser classifier from multiplicative perturbations with more non-zero weights than VAT and MLE. As we have demonstrated in Figure 3, the multiplicative perturbations reside inside a rectangle around an input x , while the additive perturbations can only lie on the ring surrounding x . As a result, there are more varieties among multiplicative perturbations than their additive counterparts, and therefore the adversarially trained DNNs need more capacity or active neurons to against multiplicative perturbations.

5. Conclusion

In this paper we propose a new type of perturbations that is multiplicative. Compared to the additive perturbations exploited by AT and VAT, the multiplicative perturbations are more perceptible and interpretable. We show that these multiplicative perturbations can be optimized via an L_0 -norm regularized objective and implemented transductively

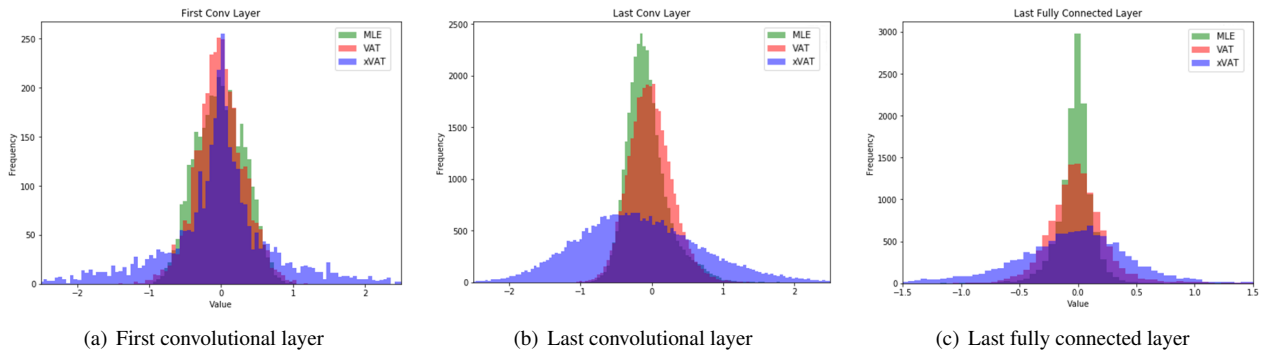


Figure 6. Histograms of the classifier weights learned by MLE, VAT and xVAT on CIFAR-100. The histograms are computed from different CNN layers.

and inductively. Thanks to the hard concrete reparameterization, the resulting algorithms xAT and xVAT are computationally more efficient than their additive counterparts. Extensive experiments on synthetic and four established image classification benchmarks demonstrate that xAT and xVAT match or outperform the state-of-the-art algorithms while being about 30% faster. Visualization of xAT and xVAT demonstrates a stark contrast to their additive counterparts.

As for future extensions, we are interested in investigating the interplay between xVAT and L_0 -norm based network sparsification [11]. Both algorithms are developed via the L_0 regularizations, while xVAT learns a dense network and L_0 -ARM [11] prunes redundant neurons. The combination of them might lead a network that is both robust and efficient.

References

- [1] Ben Athiwaratkun, Marc Finzi, Pavel Izmailov, and Andrew Gordon Wilson. There are many consistent explanations of unlabeled data: Why you should average. In *International Conference on Learning Representations (ICLR)*, 2019. 5
- [2] Thomas Bird, Julius Kunze, and David Barber. Stochastic variational optimization. *arXiv preprint arXiv:1809.04855*, 2018. 3
- [3] Yarin Gal, Jiri Hron, and Alex Kendall. Concrete dropout. In *Advances in Neural Information Processing Systems (NeurIPS)*, 2017. 7
- [4] Ian Goodfellow, Jonathon Shlens, and Christian Szegedy. Explaining and harnessing adversarial examples. In *International Conference on Learning Representations (ICLR)*, 2015. 1, 2, 5
- [5] Will Grathwohl, Dami Choi, Yuhuai Wu, Geoff Roeder, and David Duvenaud. Backpropagation through the void: Optimizing control variates for black-box gradient estimation. In *International Conference on Learning Representations (ICLR)*, 2018. 3
- [6] Geoffrey E. Hinton and Drew van Camp. Keeping the neural networks simple by minimizing the description length of the weights. In *Proceedings of the Sixth Annual Conference on Computational Learning Theory (COLT)*, 1993. 5
- [7] Eric Jang, Shixiang Gu, and Ben Poole. Categorical reparameterization with gumbel-softmax. In *International Conference on Learning Representations (ICLR)*, 2017. 3
- [8] Diederik Kingma and Jimmy Ba. Adam: A method for stochastic optimization. In *International Conference on Learning Representations (ICLR)*, 2015. 10
- [9] Alex Krizhevsky and Geoffrey Hinton. Learning multiple layers of features from tiny images. Technical report, 2009. 5, 10
- [10] Yann Lecun, Leon Bottou, Yoshua Bengio, and Patrick Haffner. Gradient-based learning applied to document recognition. In *Proceedings of the IEEE*, 1998. 5, 10
- [11] Yang Li and Shihao Ji. L_0 -ARM: Network sparsification via stochastic binary optimization. In *The European Conference on Machine Learning (ECML)*, 2019. 9
- [12] Christos Louizos, Max Welling, and Diederik P. Kingma. Learning sparse neural networks through l_0 regularization. In *International Conference on Learning Representations (ICLR)*, 2018. 3, 4
- [13] Chris J. Maddison, Andriy Mnih, and Yee Whye Teh. The concrete distribution: A continuous relaxation of discrete random variables. In *International Conference on Learning Representations (ICLR)*, 2017. 3
- [14] Takeru Miyato, Shinichi Maeda, Masanori Koyama, Ken Nakae, and Shin Ishii. Distributional smoothing by virtual adversarial examples. In *International Conference on Learning Representations (ICLR)*, 2016. 1, 2, 5, 6, 10, 11
- [15] Takeru Miyato, Shin-ichi Maeda, Masanori Koyama, and Shin Ishii. Virtual adversarial training: a regularization method for supervised and semi-supervised learning. *IEEE transactions on pattern analysis and machine intelligence*, 2018. 1, 5, 6, 7, 10, 11
- [16] Yuval Netzer, Tao Wang, Adam Coates, Alessandro

- Bissacco, Bo Wu, and Ng Andrew Y. Reading digits in natural images with unsupervised feature learning. 2011. [5](#), [10](#)
- [17] Sungrae Park, JunKeon Park, Su-Jin Shin, and Il-Chul Moon. Adversarial dropout for supervised and semi-supervised learning. In *AAAI Conference on Artificial Intelligence*, 2018. [5](#), [6](#), [11](#)
- [18] Siyuan Qiao, Wei Shen, Zhishuai Zhang, Bo Wang, and Alan Yuille. Deep co-training for semi-supervised image recognition. In *Proceedings of the European Conference on Computer Vision (ECCV)*, 2018. [5](#)
- [19] Antti Rasmus, Mathias Berglund, Mikko Honkala, Harri Valpola, and Tapani Raiko. Semi-supervised learning with ladder networks. In *Advances in Neural Information Processing Systems (NeurIPS)*. 2015. [7](#)
- [20] Mehdi Sajjadi, Mehran Javanmardi, and Tolga Tasdizen. Regularization with stochastic transformations and perturbations for deep semi-supervised learning. In *Advances in Neural Information Processing Systems (NeurIPS)*, 2016. [5](#)
- [21] Tim Salimans, Ian Goodfellow, Wojciech Zaremba, Vicki Cheung, Alec Radford, and Xi Chen. Improved techniques for training gans. In *Advances in neural information processing systems (NeurIPS)*, 2016. [7](#)
- [22] Laine Samuli and Aila Timo. Temporal ensembling for semi-supervised learning. In *International Conference on Learning Representations (ICLR)*, 2017. [5](#), [6](#), [7](#), [11](#)
- [23] Jost Tobias Springenberg. Unsupervised and semi-supervised learning with categorical generative adversarial networks. In *International Conference on Learning Representations (ICLR)*, 2015. [7](#)
- [24] Nitish Srivastava, Geoffrey Hinton, Alex Krizhevsky, Ilya Sutskever, and Ruslan Salakhutdinov. Dropout: A simple way to prevent neural networks from overfitting. *Journal of Machine Learning Research*, 2014. [1](#), [5](#), [7](#)
- [25] Christian Szegedy, Wojciech Zaremba, Ilya Sutskever, Joan Bruna, Dumitru Erhan, Ian Goodfellow, and Rob Fergus. Intriguing properties of neural networks. In *International Conference on Learning Representations (ICLR)*, 2014. [1](#)
- [26] Antti Tarvainen and Harri Valpola. Mean teachers are better role models: Weight-averaged consistency targets improve semi-supervised deep learning results. In *Advances in Neural Information Processing Systems (NeurIPS)*, 2017. [5](#), [7](#)
- [27] George Tucker, Andriy Mnih, Chris J. Maddison, John Lawson, and Jascha Sohl-Dickstein. Rebar: Low-variance, unbiased gradient estimates for discrete latent variable models. In *Advances in Neural Information Processing Systems (NIPS)*, 2017. [3](#)
- [28] Ronald J. Williams. Simple statistical gradient-

following algorithms for connectionist reinforcement learning. *Machine Learning*, 1992. [3](#)

- [29] Hongyi Zhang, Moustapha Cisse, Yann N. Dauphin, and David Lopez-Paz. Mixup: Beyond empirical risk minimization. In *International Conference on Learning Representations (ICLR)*, 2018. [1](#)

6. Appendix

6.1. Benchmark Datasets

The image classification benchmarks used in our experiments are described below:

1. MNIST [[10](#)] is a gray-scale image dataset containing 60,000 training images and 10,000 test images of the size 28×28 for 10 handwritten digits classification.
2. SVHN [[16](#)] is a street view house number dataset containing 73,257 training images and 26,032 test images classified into 10 classes representing digits. Each image may contain multiple real-world house number digits, and the task is to classify the center-most digit. These are RGB Images of the size 32×32 .
3. CIFAR-10 [[9](#)] contains 10 classes of RGB images of the size 32×32 , in which 50,000 images are for training and 10,000 images are for test.
4. CIFAR-100 [[9](#)] also has 60,000 RGB images of the size 32×32 , except that it contains 100 classes with 500 training images and 100 test images per class.

6.2. Experimental Setup

Our xAT and xVAT contains two sets of model parameters: (a) classifier parameter θ , and (b) per-image log α parameter as in the transductive implementation or generator parameter θ_g as in the inductive implementation. For the transductive implementation, we optimize log α by SGD with a learning rate of 0.001. For the inductive implementation, we found that one-layer CNN with one 3×3 filter works well for all our experiments, and we optimize the generator by using Adam [[8](#)] with a fixed learning rate of $1e-6$ or $2e-6$.

As for classifier parameter θ , different network architectures are used for different image classification benchmarks. In all our experiments, we use $\lambda = 1, \eta = 1$ for xVAT, and $\lambda = 1, \eta = 0.5$ for xAT.

MNIST We use an MLP with four hidden layers of 1200, 600, 300 and 150 units, respectively, for the MNIST experiments. The same MLP architecture is used for supervised training and semi-supervised training as in VAT [[14](#), [15](#)]. The input images are linearly normalized to the range of $[-0.5, 0.5]$. We use the Adam optimizer [[8](#)] with an initial

learning rate of 0.002, which is decayed by 0.9 at every 500 iterations. We train the classifier for 50,000 iterations, and at each iteration a mini-batch of 100 labeled images and 250 unlabeled images is used for training.

CNN Architecture for SVHN, CIFAR-10/100 On these three benchmarks, for the purpose of fair comparisons, we use the CNN architecture shown in Table 6, which is the same as the one used in [15, 17, 22].

Table 6. The CNN architecture used on SVHN, CIFAR-10, and CIFAR-100.

Name	Description
Input	Image
Conv1a	128 filters, 3×3 , Pad='same', LReLU($\alpha = 0.1$)
Conv1b	128 filters, 3×3 , Pad='same', LReLU($\alpha = 0.1$)
Conv1c	128 filters, 3×3 , Pad='same', LReLU($\alpha = 0.1$)
Pool1	Maxpool 2×2 pixels, Stride 2
Drop1	Dropout, $p = 0.5$
Conv2a	256 filters, 3×3 , Pad='same', LReLU($\alpha = 0.1$)
Conv2b	256 filters, 3×3 , Pad='same', LReLU($\alpha = 0.1$)
Conv2c	256 filters, 3×3 , Pad='same', LReLU($\alpha = 0.1$)
Pool2	Maxpool 2×2 pixels, Stride 2
Drop2	Dropout, $p = 0.5$
Conv3a	512 filters, 3×3 , Pad='valid', LReLU($\alpha = 0.1$)
Conv3b	256 filters, 1×1 , Pad='same', LReLU($\alpha = 0.1$)
Conv3c	128 filters, 1×1 , Pad='same', LReLU($\alpha = 0.1$)
Pool3	Global average pool, $6 \times 6 \rightarrow 1 \times 1$
Dense	Fully connected $128 \rightarrow 10$
Output	Softmax

We follow the same normalization schemes of VAT on these three benchmarks. We normalize the SVHN images to the range of $[0, 1]$. For CIFAR-10 and CIFAR-100, we normalize the images with ZCA, based on training set statistics, the same as in VAT [14, 15].

In semi-supervised learning, we train the classifier for 50000 iterations on SVHN, 200000 iterations on CIFAR-10, and 120000 iterations on CIFAR-100. At each iteration, we sample a mini-batch of 32 labeled images and 128 unlabeled images. We use the Adam optimizer with an initial learning rate of 0.001 and decay the learning rate linearly at the $[35000, 180000, 80000]$ -th iterations.

For supervised learning on CIFAR-10 and CIFAR-100, we train the CNN classifier for 300 epochs with a batch size of 100. We again use Adam with an initial learning rate of 0.003 for xAT and 0.001 for xVAT. We linearly decay the learning rate at the 2nd half of training.

6.3. Hyperparameter Tuning

Figure 7 shows the results of hyperparameter tuning of λ (Eq. 11) and η (Eq. 13) on the MNIST dataset. As we

can see, $\lambda = 1$ and $\eta = 1$ yields very competitive classification accuracies. Similar results are observed on the other benchmarks. We therefore use $\lambda = 1$ and $\eta = 1$ in all our semi-supervised learning tasks.

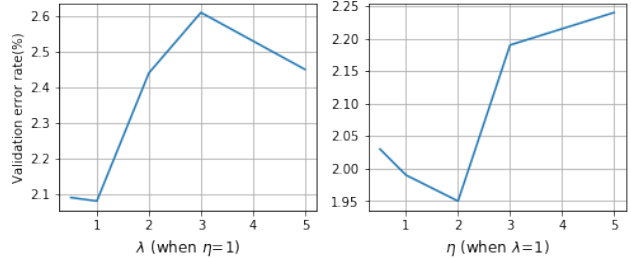


Figure 7. Hyperparameters tuning of λ and η on the MNIST dataset.